Escape of a forced-damped particle from weakly nonlinear truncated potential well

Escape of a forced-damped particle from weakly nonlinear truncated potential well

M. Farid[1,2], O. V. Gendelman[2]

[1] Department of Mechanical Engineering, Massachusetts Institute of Technology, 77 Massachusetts Ave., Cambridge, MA 02139

[2] Faculty of Mechanical Engineering, Technion – Israel Institute of Technology, Haifa, 3200003, Israel

*contacting author, faridm@mit.edu

Keywords: potential well; escape; transient processes; resonance manifold; damping.

Abstract

Escape from a potential well is an extreme example of transient behavior. We consider the escape of the harmonically forced particle under viscous damping from the benchmark truncated weakly nonlinear potential well. Main attention is paid to most interesting case of primary 1:1 resonance. The treatment is based on multiple-scales analysis and exploration of the slow-flow dynamics. Contrary to Hamiltonian case described in earlier works, in the case with damping the slow-flow equations are not integrable. However, if the damping is small enough, it is possible to analyze the perturbed slow-flow equations. The effect of the damping on the escape threshold is evaluated in an explicit analytic form. The substantial difference between the linear and weakly nonlinear cases in terms of the slow-flow dynamics of the escape mechanisms is demonstrated and discussed.

Keywords: escape; transient processes; potential well; resonance manifold; multiple scales analysis.

List of symbols

q - Non-dimensional coordinate

$U(q)$ - Weakly nonlinear truncated potential well

q_a, q_b - Displacement values which correspond to the left and right edges of the well, respectively

ε - Small parameter

α, β - Coefficients of the quadratic and cubic nonlinearities, respectively

τ - Non-dimensional time variable

Λ - Rayleigh dissipation function

λ - Damping coefficient

f, Ω, Ψ - Forcing amplitude, frequency and phase, respectively

$T_j = \varepsilon^j \tau$ - The jth non-dimensional time scale

d_j - Derivation operator with respect to time scale T_j

q_j - The jth order term in the Taylor series of the system's approximate solution

i - Unit imaginary number

A, $\bar{A}$ - Slow-varying amplitude of q_0 and its complex conjugate, respectively

σ - Detuning parameter

a, θ - Slow-varying polar amplitude and phase, respectively

γ - Slow-varying phase variable

B - Slow-varying imaginary variable

f_{cr} - Critical value of forcing amplitude

$\rho = \lambda/2\sigma$ - Detuning parameter with respect to the dip of the escape curve

$\bar{T_1}$ - The instance in slow time scale associated with the critical forcing amplitude f_{cr}

$z = \sigma \bar{T_1}$ - Transformed rescaling parameter

δ_1, δ_2 - Arbitrary small perturbations

$\tau_j = \varepsilon^{j/2}\tau$ - The jth non-dimensional time scale

D_j - Derivation operator with respect to time scale τ_j

H - Integral of motion/conservation law of the corresponding integrable system

H_0 - Initial conditions-related value of the integral of motion, H

D - Simplified conservation law, obtained by ignoring the trivial solution of the system

η - Parameter that expresses the competition between the softening and the hardening effects of the quartic and cubic nonlinearities, respectively

a_S, $f_{cr,S}$ - Slow-varying amplitude and critical forcing amplitude associated with the 'saddle mechanism'

$f_{cr,M}$ - Critical forcing amplitude associated with the 'maximum mechanism'

σ^*, f_{cr}^* - Detuning and critical forcing amplitude associated with coexistence of both 'saddle mechanism' and 'maximum mechanism'

a_0, γ_0 - The slow-varying polar amplitude and phase variable associated with the solution of the undamped case and the limiting phase trajectory (LPT), i.e. zero initial conditions

a_M, γ_M - The slow-varying polar amplitude and phase variable associated with the 'maximum mechanism'

$a_{l,j}$, $\gamma_{l,j}$, $f_{cr,l,j}$, $l = S, M$, $j = 0, 1$ - First and second order approximation terms of the slow-varying polar amplitude, slow-varying phase variable, and critical forcing amplitude, associated with the saddle and maximum mechanisms, with respect to small damping coefficient $\varepsilon\lambda$, respectively

2

K, **E**, **Π** - Complete elliptic integrals of the first, second and third kind, respectively

1. Introduction

Escape from a potential well is a classic and common problem which arises in various fields, such as chemistry, physics and engineering [1]–[7]. Different excitations may lead to escape from a potential well, including stochastic [8], [9], impulsive loading [10], [11], harmonic forcing [2] and others.

The relation between the amplitude to the frequency of the periodic excitation is usually referred to as escape curve, which normally exhibits a sharp minimum in the vicinity of the particle's natural frequency [1], [2], [12]–[14].

It was demonstrated that the transient escape processes, which correspond to the primary resonance can be explored and describes with the help of 1:1 resonance manifold (RM). The latter represents the phase portrait of the slow-flow of the system. The trajectory of the RM on which the system will flow is determined by its initial conditions. The trajectory which corresponds to zero initial conditions is referred to as limiting phase trajectory (LPT, [15]–[18]). Escape from the potential well is achieved when the LPT reaches a critical threshold, bringing the system to the edge of the well.

Previous studies [19]–[22] have shown that the sharp 'dip' in the escape curve corresponds to intersection between two escape graphs which are associates with two distinguished competing escape mechanisms, originated from the nonlinear features of the well. The former, corresponds to transition of the LPT trough a saddle point of the RM before reaching the escape boundary of the well, and hence called 'saddle mechanism'. The latter, corresponds to direct motion of the LPT towards the upper bound of the RM, and referred to as 'maximum mechanism'.

The results mentioned above heavily relied on integrability of the slow-flow equations for approximation of isolated resonance in forced single-DOF oscillator [23]. Damping destroys the integrability, and therefore analysis of the escape curves for the damped systems requires more complicated tools. Paper [20] provided certain numeric insight into this issue; however, the effect of the damping on both shape and location of the escape curves and on the underlying dynamical mechanisms still lacks appropriate understanding.

In the current paper, models of linear and weakly nonlinear truncated wells, first described in paper [21], are re-visited, in order to analyze the contribution of damping with the help of appropriate analytical and numerical tools.

Section 2 is devoted to the description of the model. In Section 3, the escape mechanisms of the corresponding linear damped system are explored with the help of asymptotical tools. The analytical results are verified numerically. In Section 4, the case of an over-damped particle in a purely-parabolic potential well is considered, and in Section 5, the dynamics of a weakly-damped particle in a nonlinear potential well is examined. The relations between the shape of the escape curve, the system's nonlinearities and the damping are explored in details.

2. Model description

The simplest model that captures the essence of the escape phenomenon of a particle in a truncated linear potential well with nonlinear perturbations is considered.

$$U(q) = \begin{cases} -\dfrac{1}{2} + \dfrac{q^2}{2} - \dfrac{\varepsilon\alpha}{3}q^3 - \dfrac{\varepsilon^2\beta}{4}q^4 & q \in (q_a, q_b) \\ 0 & else \end{cases} \qquad (1)$$

Here q is a non-dimensional coordinate, ε is a small parameter, and α and β are coefficients of order unity. Terms q_a and q_b are the displacement values which correspond to the left and right edges of the well, respectively. The nonlinear perturbations taken are up to forth order, so the contributions of both symmetric and asymmetric nonlinearities are focused, as shown in Figure 1:
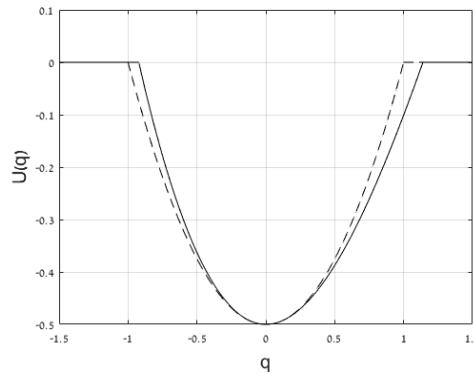

Figure 1- Sketch of the perturbed truncated parabolic potential well corresponding to Equation (1), solid-line: parabolic potential well with quartic and cubic perturbations, dashed-line: pure parabolic potential well, for: $\varepsilon = 0.1, \alpha = 2.95, \beta = 1$

The particle escapes the well when $U(q) = 0$. However, this criterion is not very convenient for implementation. Hence, one can adopt the following escape criterion in first approximation with respect to the linear case:

$$\max_{\tau} |q(\tau)| = 1 \tag{2}$$

We introduce a small linear damping using the following Rayleigh dissipation function:

$$\Lambda = \frac{1}{2} \varepsilon \lambda \dot{q}^2 \tag{3}$$

Here, λ is a damping coefficient of order unity. Thus, the non-dimensional equation of motion of the particle is as follows:

$$\ddot{q} + \varepsilon \lambda \dot{q} + q - \sqrt{\varepsilon}\, \alpha q^2 - \varepsilon \beta q^3 = \varepsilon f \cos(\Omega \tau + \Psi) \tag{4}$$

Here f, Ω and Ψ are forcing amplitude, frequency and phase of order unity, respectively, and dot stands for differentiation with respect to non-dimensional time τ.

3. Linear potential well

In the following section, a classical under-damped particle in a linear potential well is considered. Its equation of motion is obtained by neglecting the nonlinear perturbations in Equation (4), i.e. taking $\alpha = \beta = 0$:

$$\ddot{q} + \varepsilon \lambda \dot{q} + q = \varepsilon f \cos(\Omega \tau + \Psi) \tag{5}$$

Since the system is under-damped, the escape is governed by an overshoot phenomenon. Hence, steady state analysis will not describe the relevant dynamical regime, and detailed analysis of the transient response is required.

3.1. Analytical treatment

Even though the system is linear and hence solvable, we are interested not only in its analytical solution, but specifically the conditions which lead to escape of the particle from the well, i.e. transient growth of the oscillations amplitude up to unity. The system is considered in the vicinity of main resonance. Multiple scales approach is applied to seek an approximate solution of the following form:

$$q(\tau) \approx q_0(T_0, T_1) + \varepsilon q_1(T_0, T_1) \tag{6}$$

Here $T_j = \varepsilon^j \tau$. Equation (6) is substituted into Equation (5), and two leading terms are collected as follows:

$$
\begin{aligned}
d_0^2 q_0 + q_0 &= 0 \\
d_0^2 q_1 + q_1 &= -2 d_0 d_1 q_0 - \lambda d_0 q_0 + f \cos(\Omega T_0 + \Psi)
\end{aligned}
\tag{7}
$$

Here $d_j = \partial / \partial T_j$. The solution of the first equation in Equation (7) is as follows:

$$q_0(T_0, T_1) = A(T_1) e^{iT_0} + c.c. \tag{8}$$

Here i is the unit imaginary number. Substituting the first order solution in Equation (8) to the next order equation in Equation (7):

$$d_0^2 q_1 + q_1 = -2i\left(A' e^{iT_0} - c.c.\right) - i\lambda\left(A e^{iT_0} - c.c.\right) + \frac{f}{2}\left(e^{i(\Omega T_0 + \Psi)} + c.c.\right) \tag{9}$$

In the current section, tag stands for derivation with respect to slow time scale T_1. Detuning parameter σ is introduced, as follows:

$$\Omega = 1 + \varepsilon \sigma \tag{10}$$

Polar transformation and new phase variable are adopted:

$$A(T_1) = \frac{1}{2} a(T_1) e^{i\theta(T_1)}, \quad \gamma(T_1) = \sigma T_1 + \Psi - \theta(T_1) \tag{11}$$

After substituting Equations (10)-(11) to Equation (9), and dividing it to real and imaginary equations, we yield the slow evolution equations of the system:

$$
\begin{aligned}
a' &= -\frac{\lambda}{2} a + \frac{f}{2} \sin \gamma \\
a\gamma' &= \sigma a + \frac{f}{2} \cos \gamma
\end{aligned}
\tag{12}
$$

In order to reduce the order of the system to a single imaginary equation, we introduce the following imaginary variable:

$$B(T_1) = a(T_1) e^{-\gamma(T_1)} \tag{13}$$

We substitute Equation (13) into Equation (12) and obtain the following equation:

$$B' + \left(i\sigma + \frac{\lambda}{2}\right) B = -\frac{i}{2} f \tag{14}$$

The solution of Equation (14) is as follows:

$$B\left(T_1\right) = \frac{if}{2\sigma i + \lambda}\left(e^{-\left(i\sigma + \frac{\lambda}{2}\right)T_1} - 1\right) \tag{15}$$

We recall the escape criterion:

$$\left|q\left(\tau\right)\right| = \frac{f}{\sqrt{4\sigma^2 + \lambda^2}}\sqrt{e^{-\lambda T_1} + 1 - 2e^{-\frac{\lambda}{2}T_1}\cos\left(\sigma T_1\right)} = 1 \tag{16}$$

The critical value of forcing amplitude with respect to a specific value of σ is given by the following expression:

$$f_{cr} = \frac{\sqrt{4\sigma^2 + \lambda^2}}{\sqrt{\max\left(e^{-\lambda T_1} + 1 - 2e^{-\frac{\lambda}{2}T_1}\cos\left(\sigma T_1\right)\right)}} \tag{17}$$

Maximizing the denominator is obtained by eliminating its derivative, which yield the following equation:

$$e^{-\frac{\lambda}{2}\overline{T_1}} = \frac{1}{\rho}\sin\left(\sigma\overline{T_1}\right) + \cos\left(\sigma\overline{T_1}\right) \tag{18}$$

Here $\rho = \lambda/2\sigma$, and $\overline{T_1}$ is the instance in which the denominator in Equation (17) reaches maximum. Let us substitute Equation (18) into Equation (17):

$$f_{cr} = \frac{\lambda}{\left|\sin\left(z\right)\right|}, \ z = \sigma\overline{T_1} \tag{19}$$

As one can conclude from Equation (19), $\overline{T_1}$ cannot be obtained explicitly. Numerical investigation with respect to damping and detuning parameters λ and σ is shown in Figure 2:
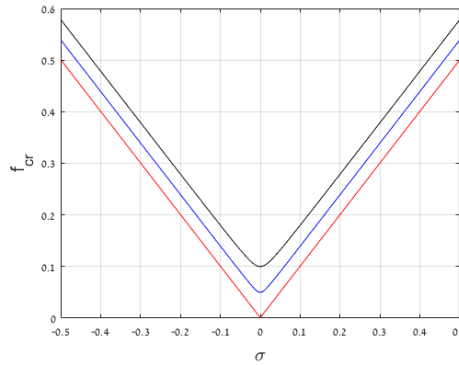

Figure 2- Escape curves using numerical integration of Equations (18)-(19), red: $\lambda = 0.001$, blue: $\lambda = 0.05$, black: $\lambda = 0.1$.

One can see in Figure 2 that in contrast to the corresponding nonlinear case explored in the previous studies [24], the escape curve of the linear case has a smooth minimum, and thus it is not associated with intersection of two distinguished branches related to different escape mechanisms.

In the following Section, we explore explicit asymptotic approximations for Equations (18)-(19), near and far from the minimum of the curve.

3.1.1. Vicinity of the minimum, $\rho \gg 1$

We expand Equation (19) to a Taylor series near the minimum with respect to small parameter $1/\rho$:

$$f_{cr}\left(z = \pi/2 + 1/\rho\right) \approx \lambda\left(1 + 2\left(\frac{\sigma}{\lambda}\right)^2\right) \tag{20}$$

One can see that the parabolic characteristics of the curve, shown in Figure 2, are captured in expression (20).

3.1.2. Far from the minimum, $\rho \ll 1$

According to (19), time instance $\overline{T}_1$ equals to the ratio of variable z and detuning parameter σ. Hence, z and σ must have the same sign.

For $z > 0$, i.e. $\rho > 0$, we expand Equation (18) to Taylor series in the vicinity of $z = \pi$ with respect to an arbitrary small perturbation: $z = \pi + \delta_1(\rho)$. After collecting the leading terms, the following expression is obtained:

$$\delta_1(\rho) = -2\rho + \pi\rho^2 + O\left(\rho^2\right) \tag{21}$$

We expand Equation (19) with respect to a small perturbation in Equation (21) to obtain the following approximated expression:

$$f_{cr} \approx \sigma + \lambda\frac{\pi}{4} \tag{22}$$

Now for $z < 0$, i.e. $\rho < 0$, we expand Equation (18) to a Taylor series in vicinity of $z = -\pi$ with respect to an arbitrary small perturbation: $z = -\pi + \delta_2(\rho)$. After collecting the leading order terms, the following expression is obtained:

$$\delta_2(\rho) = -2\rho - \pi\rho^2 + O\left(\rho^2\right) \tag{23}$$

We expand Equation (19) with respect to the perturbation in Equation (23), and obtain the following expression:

$$f_{cr} \approx |\sigma| + \lambda\frac{\pi}{4} \tag{24}$$

Therefore, from Equations (22), (24) one can see that the generic approximate expression for the critical forcing amplitude is given by Equation (24). Thus, the limit of no damping is indeed restored. However, the presence of two different limits, as well as modification of smoothness of the curve $f_{cr}(\lambda, \sigma)$, point on somewhat unexpected singular character of the limit $\lambda \to 0$. In the next Section, the approximate results are verified by numeric simulations.

3.2. Numerical verification

Comparisons between numerical solutions of Equation (18) and the corresponding asymptotic approximations, for both small and large detuning values, are presented in Figure 3.
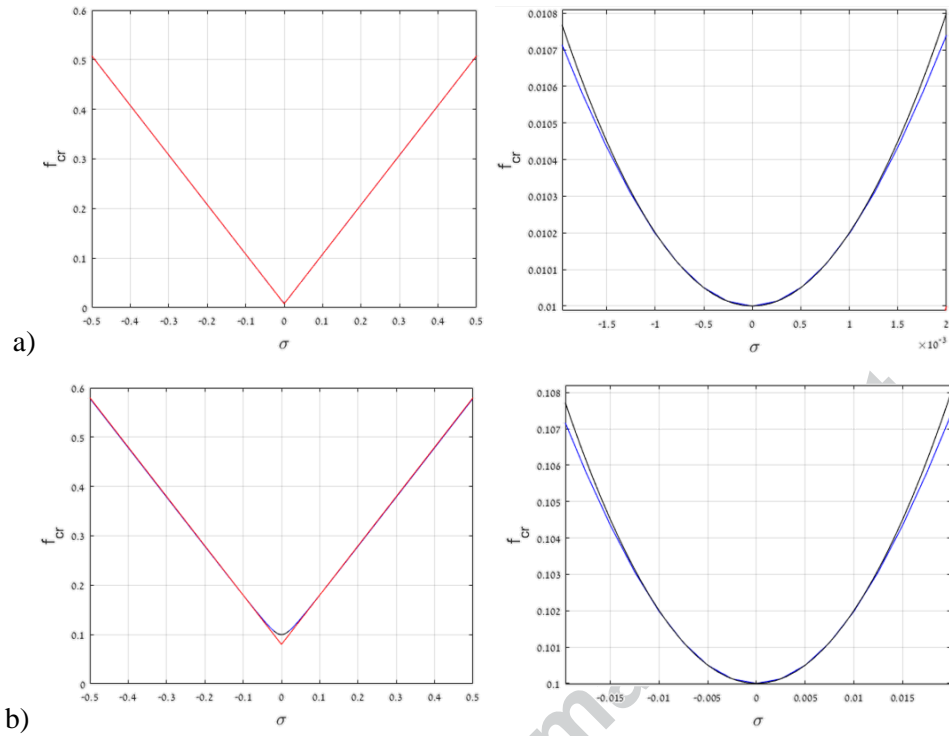

Figure 3- Comparison between numerical integration of Equation (18) (black line), and both asymptotic approximations, i.e. Equation (20) for $\rho \gg 1$, and Equation (24) for $\rho \ll 1$ (blue and red, respectively); a) $\lambda = 0.01$, b) $\lambda = 0.1$; left: $\sigma \in (-0.5, 0.5)$, right: zoom-in near the minimum.

One can see in Figure 3, that the approximation for $\rho \gg 1$ is valid for $|\sigma| < 0.2\lambda$, and the approximation for $\rho \ll 1$ is valid for $|\sigma| > 0.5\lambda$. Moreover, we see in Figure 3 (a) a clear convergence to the escape curve shown by [21] for the undamped linear potential well.

In Figure 4, the asymptotic results obtained above, are verified numerically by integration of the original equation of motion, shown in Equation (5).
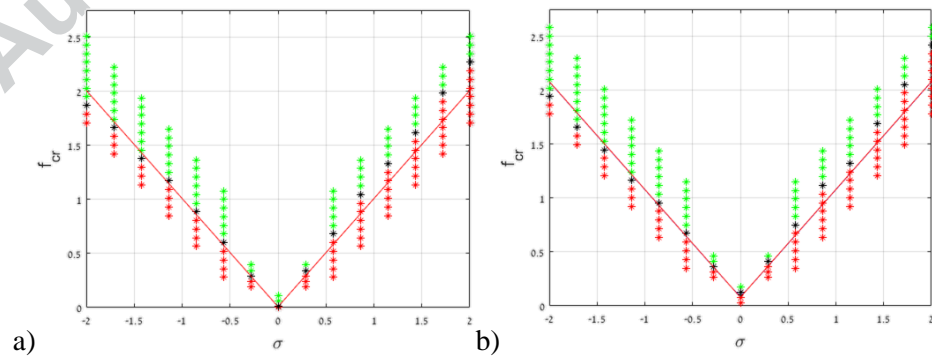

Figure 4- comparison between the asymptotic approximation of the escape curve (red solid line) and numerical results, red points: no escape, green points: escape, black points: escape threshold; a) $\lambda = 0.01$, b) $\lambda = 0.1$.

One can see that the numerical results shown in Figure 4 are in good agreement with the approximated curves. In order to investigate the escape mechanism, numerical simulations of the equation of motion shown in Equation (5) were conducted, as shown in Figure 5.
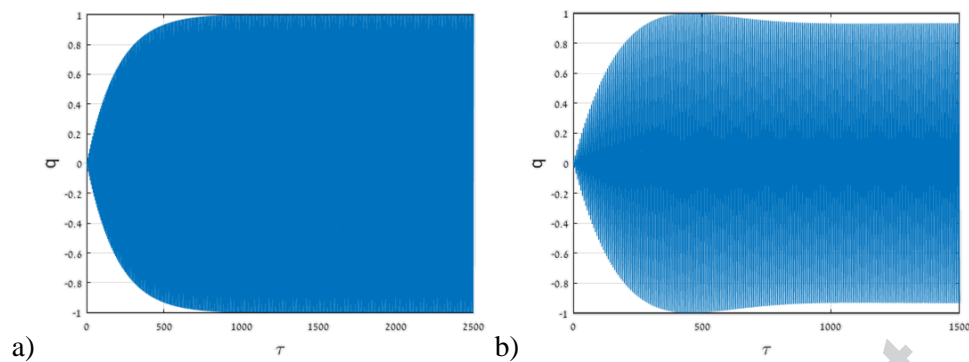

Figure 5- Numerical simulations demonstrating the characteristic escape mechanism on the escape threshold near and far from the minimum of the escape curve, for $\varepsilon = 0.1$, $\lambda = 0.1$, a) $\sigma = 0.01, f = 0.1025$, b) $\sigma = 0.05, f = 0.1325$

Near the minimum of the curve, i.e. for small values of σ and f, the escape mechanism is characterized by a gradually growing amplitude which converges to unity, as shown in Figure 5 (a). Hence, this escape mechanism will be referred to as 'steady-state mechanism'. On the other hand, for larger detuning and forcing values, overshoot phenomenon becomes more significant and governs the escape process, as shown in Figure 5(b). Thus, this escape mechanism will be called 'transient mechanism'. Even farther from the minimum, the dominance of overshoot increases, when escape can take place even during the first oscillation periods, as shown in Figure 6.
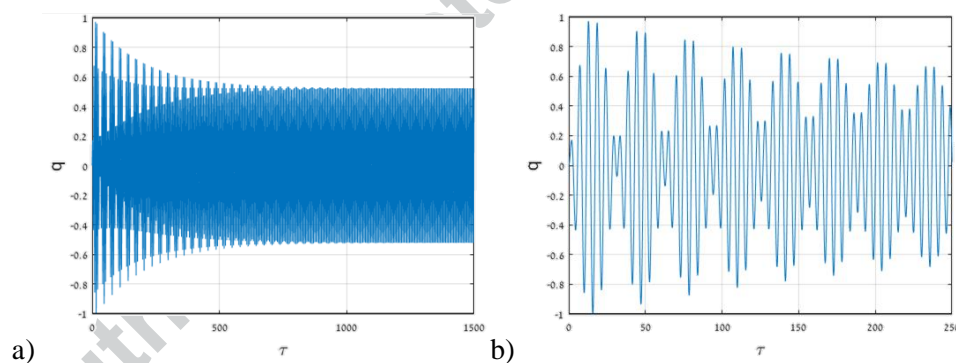

Figure 6- Numerical simulations demonstrating the characteristic escape mechanism taking place far from the minimum of the escape curve, a) for $\lambda = 0.1$, $\varepsilon = 0.1$, $\sigma = 2, f = 2.3$, corresponding to small deviation below the escape curve; b) zoom-in.

Recalling the transient escape processes arise in both linear and non-linear under-damped systems, it is clear that the simplest escape process takes place for an over-damped particle subjected to purely parabolic potential well. In this case, overshoot is suppressed, and escape will be governed merely by stead-state mechanisms. Thus, it can be described only by steady state analysis.

4. Escape of the overdamped particle from a linear potential well

For the sake of generality and completeness, the linear overdamped case is now analyzed. In this case, the underlying (steady-state) escape mechanisms are described with the help of analytical tools. Then, the analytical results are verified numerically.

4.1. Analytical treatment

From Equation (5), the equation of motion of the forced-damped linear oscillator is as follows:

$$\ddot{q} + \lambda \dot{q} + q = f \cos\left(\Omega \tau + \Psi\right) \tag{25}$$

Here, the excitation frequency is taken as: $\Omega = 1 + \sigma$. The corresponding response amplitude is given by the following expression:

$$A = \frac{f}{\sqrt{\sigma^2 \left(2 + \sigma\right)^2 + \lambda^2 \left(1 + \sigma\right)^2}} \tag{26}$$

Since the escape is governed by steady-state response, the escape criterion is $A = 1$. Hence, the escape curve is obtained by the following equation:

$$f_{cr} = \sqrt{\sigma^2 \left(2 + \sigma\right)^2 + \lambda^2 \left(1 + \sigma\right)^2} \tag{27}$$

It is easy to show that a pitchfork bifurcation occurs for $\lambda = \sqrt{2}$, when the escape curve associated with Equation (27) shifts from having a local maximum at $\sigma = -1$ and two additional global minima, to having a single global minimum at $\sigma = -1$. However, numerical simulations show that over-damped oscillations take place for $\lambda > 2$. Thus, the current section will focus on damping coefficient in the range $\lambda > 2$, i.e. the case of a single global minimum at $\sigma = -1$.

4.2. Numerical verification

In Figure 7, we verify the analytical expression in Equation (27) using direct numerical integrations of the particle's equation of motion in Equation (25).
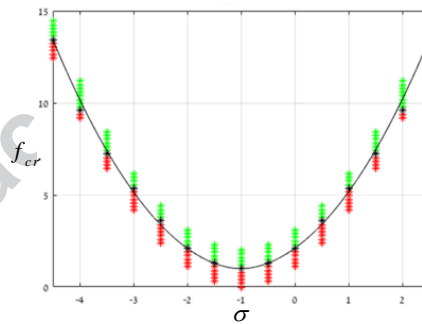

Figure 7- escape curve of an over-damped linear oscillator - analytical prediction (solid black line) vs. numerical verifications (red point: no escape, green point: escape, black point: escape threshold), for $\varepsilon = 0.1, \quad \lambda = 2.1$.

As one can see in Figure 7, the numerical results are in good agreement with the analytical predictions. A small bias in the results is caused due to a slight over-shoot, demonstrated in Figure 8 (b). The overshoot corresponds to the homogenous part of the solution, which decays faster for high damping.
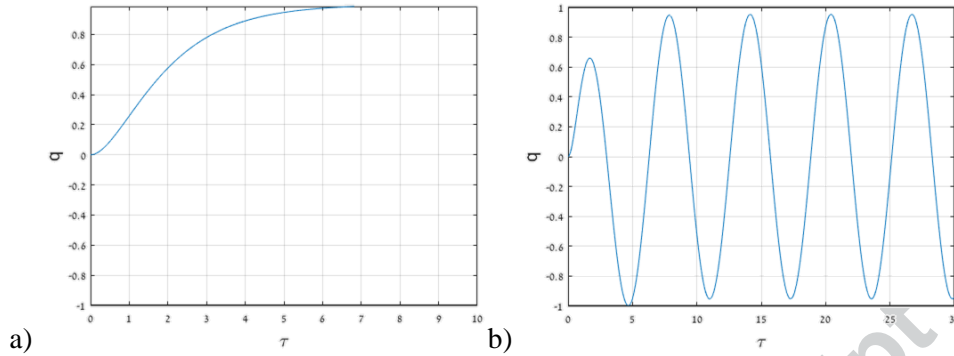

a) b)

Figure 8- Numerical simulations both near and far from the minimum of the escape curve; for $\varepsilon = 0.1$ and $\lambda = 2.1$ a) $\sigma = -1$, $f = 1$ b) $\sigma = 0$, $f = 2$.

As one can learn from Figure 8, near the minimum of the escape curve, over-damped response is obtained. However, farther from the minimum, oscillations take place due to larger forcing amplitude, f_{cr}.

5. Weakly nonlinear potential well

In the following section, several analytical approaches are applied in order to analyze the structure of the RM of the weakly nonlinear system in Equation (4), and to describe its escape mechanisms.

5.1. Analytical treatment

5.1.1. Multiple scales analysis

Following [25], we seek an approximate solution from the following form:

$$q(\tau) \approx q_0(\tau_0, \tau_1, \tau_2) + \sqrt{\varepsilon} q_1(\tau_0, \tau_1, \tau_2) + \varepsilon q_2(\tau_0, \tau_1, \tau_2) \tag{28}$$

Here $\tau_i = \varepsilon^{i/2}\tau$. Detuning parameter σ is adopted according to Equation (10). Substituting Equations (10), (28) to Equation (4) and collecting terms of similar orders, yields the following set of equations:

$$
\begin{aligned}
O(1): \quad & D_0^2 q_0 + q_0 = 0 \\
O(\sqrt{\varepsilon}): \quad & D_0^2 q_1 + q_1 = -2 D_0 D_1 q_0 + \alpha q_0^2 \\
O(\varepsilon): \quad & D_0^2 q_2 + q_2 = -2 D_0 D_1 q_1 - 2 D_0 D_2 q_0 - D_1^2 q_0 - \lambda D_0 q_0 \\
& \qquad\qquad + 2\alpha q_0 q_1 + \beta q_0^3 + f\cos(\tau_0 + \Psi + \sigma\tau_2)
\end{aligned}
\tag{29}
$$

Here $D_j = \partial/\partial\tau_j$. The general solution of the first equation in Equation (29) is as follows:

$$q_0 = A(\tau_1, \tau_2) e^{i\tau_0} + \overline{A}(\tau_1, \tau_2) e^{-i\tau_0} \tag{30}$$

Here $\overline{A}$ refers to the complex conjugate of the slow-varying amplitude A. Substituting Equation (30) into the second equation in Equation (29) yields:

$$D_0^2 q_1 + q_1 = -2 D_1 A e^{i\tau_0} + \alpha \left(A^2 e^{2i\tau_0} + A\overline{A} \right) + c.c. \tag{31}$$

Eliminating the secular terms in Equation (31) yields the following expression:

$$D_1 A = 0 \rightarrow A = A\left(\tau_2\right) \tag{32}$$

We substitute expression (32) into Equation (31), solve the resulting equation, and obtain the following term:

$$q_1 = -\alpha \left(-2 A\overline{A} + \frac{1}{3} A^2 e^{2i\tau_0} + \frac{1}{3} \overline{A}^2 e^{-2i\tau_0} \right) \tag{33}$$

Substituting Equations (30) and (33) into the third equation of Equation (29):

$$D_0^2 q_2 + q_2 = -\left(2i \left(A' + \frac{\lambda}{2} A \right) - \left(3\beta + \frac{10\alpha^2}{3} \right) A^2 \overline{A} + \frac{1}{3} f e^{i(\sigma\tau_2 + \Psi)} \right) e^{i\tau_0} + c.c. + N.S.T. \tag{34}$$

Here, c.c. refers to the complex conjugate of the previous term, and N.S.T. (Non Secular Terms) stands for terms proportional to $\exp\left(\pm 3i\tau_0\right)$. In the current section, tag stands for derivation with respect to super-slow time scale τ_2. Let us introduce the following polar substitution and ansatz:

$$A\left(\tau_2\right) = \frac{1}{2} a\left(\tau_2\right) e^{i\theta(\tau_2)}, \ \gamma = \sigma\tau_2 + \Psi - \theta \tag{35}$$

After applying ansatz (35) on Equation (34), and separating the real and imaginary terms, we yield the slow evolution equation of the system:

$$
\begin{aligned}
a' &= -\frac{\lambda}{2} a + \frac{f}{2} \sin\gamma \\
a\gamma' &= a\sigma + 4\eta a^3 + \frac{f}{2}\cos\gamma; \quad \eta = \frac{9\beta + 10\alpha^2}{96}
\end{aligned}
\tag{36}
$$

Hence, the third order approximation of the solution is as follows:

$$q(\tau) = a\cos\left(\Omega\tau - \theta\right) - \frac{1}{2}\sqrt{\varepsilon}\,\alpha\, a^2 \left(-1 + \frac{1}{3}\cos\left(2\Omega\tau - 2\theta\right) \right) + O\left(\varepsilon\right) \tag{37}$$

Consequently, the escape criterion can be taken as follows:

$$\max_{\tau} \left| q\left(\tau\right) \right| = a + O\left(\sqrt{\varepsilon}\right) = 1 \tag{38}$$

Following [15], it is obvious that system (36) is integrable for zero damping. The corresponding integral of motion/conservation law of this case is presented the following form:

$$H = a \left(\frac{9\beta + 10\alpha^2}{96} a^3 + \frac{\sigma}{2} a + \frac{f}{2}\cos\gamma \right) \tag{39}$$

In the conservative case we get $H = H_0$, where H_0 depends on initial conditions, and in the case of zero initial conditions one obtains $H_0 = 0$. The trajectory in phase plane, which corresponds to

zero initial conditions is called the limiting phase trajectory (LPT). Hence, and by ignoring the trivial solution of Equation (39), the conservation law can be simplified to the following form:

$$D = \eta\, a^3 + \frac{\sigma}{2} a + \frac{f}{2} \cos \gamma\,; \ \eta = \frac{9\beta + 10\alpha^2}{96} \tag{40}$$

Here, parameter η expresses the competition between the softening and the hardening effects of the quartic and cubic terms, respectively. The first expression in Equation (40) is further used for the exploration of the transient dynamics on the RM. The trajectories of the RM correspond to different values of D. As mentioned above, farther analysis will focus on the dynamics of a particle starting from rest, i.e. $D = 0$, which correspond to the LPT.

Let us find explicit expressions for the critical escape values of detuning and forcing coefficients, corresponding to the Hamiltonian case. First escape scenario occurs when the LPT passes through a saddle point on the RM, located in $(\gamma, a) = (0, a_s)$, before reaching the upper boundary of the well. Thus, this escape mechanism will be referred to as the 'saddle mechanism'.

$$D\left(f = f_{cr,S}, a = a_s, \gamma = 0\right) = 0 \rightarrow \boxed{a_s = \sqrt{\frac{-\sigma}{6\eta}}}$$

$$\left.\frac{\partial D}{\partial a}\right|_{\gamma = 0} = 0 \rightarrow \boxed{f_{cr,S} = \frac{2}{3\sqrt{6\eta}} (-\sigma)^{\frac{3}{2}}} \tag{41}$$

The second scenario occurs when the LPT directly reaches the boundary of the well, located in $(\gamma, a) = (\pi, 1)$, without crossing any stationary point on the RM. Hence, this mechanism will be referred to as the 'maximum mechanism'

$$D\left(f = f_{cr,M}, a = 1, \gamma = \pi\right) = 0 \rightarrow \boxed{f_{cr,M} = \sigma + 2\eta} \tag{42}$$

The intersection between both curves corresponds to the co-existence of both mechanisms, which corresponds to the following parameters set:

$$f_{cr,S} = f_{cr,M} \rightarrow \boxed{\sigma^* = -\frac{3}{2}\eta, \ f_{cr}^* = \frac{1}{2}\eta} \tag{43}$$
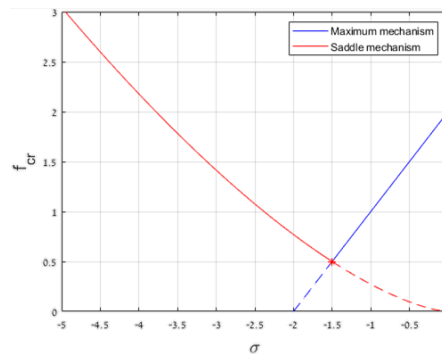

Figure 9- Theoretical prediction of the escape threshold. Blue and red dashed lines correspond to maximum and saddle escape mechanisms, respectively. Solid lines represent the resulting escape curve, and dashed lines mean that the corresponding escape mechanism is overruled by the other one. Red point correponds to the intersection between two curves, i.e. coexsistance of both mechanisms; for parameters: $\varepsilon = 0.1, \eta = 1$.

As one can see in Figure 9, the minimum of the escape curve is shifted due to the presence of the nonlinear perturbations. The shift size and direction is defined by parameter η .

As explained in previous studies [20], [21], [24], each branch in the diagram shown in Figure 9 represents a different escape mechanism. The red branch represents the 'maximum mechanism' (see Figure 10 (a)), and the blue branch represents the 'saddle mechanism' (see Figure 10 (c)). The intersection point of both branches, describes the coexistence of both mechanisms, when the LPT passes through the saddle and tangents to the escape boundary (see Figure 10 (b))
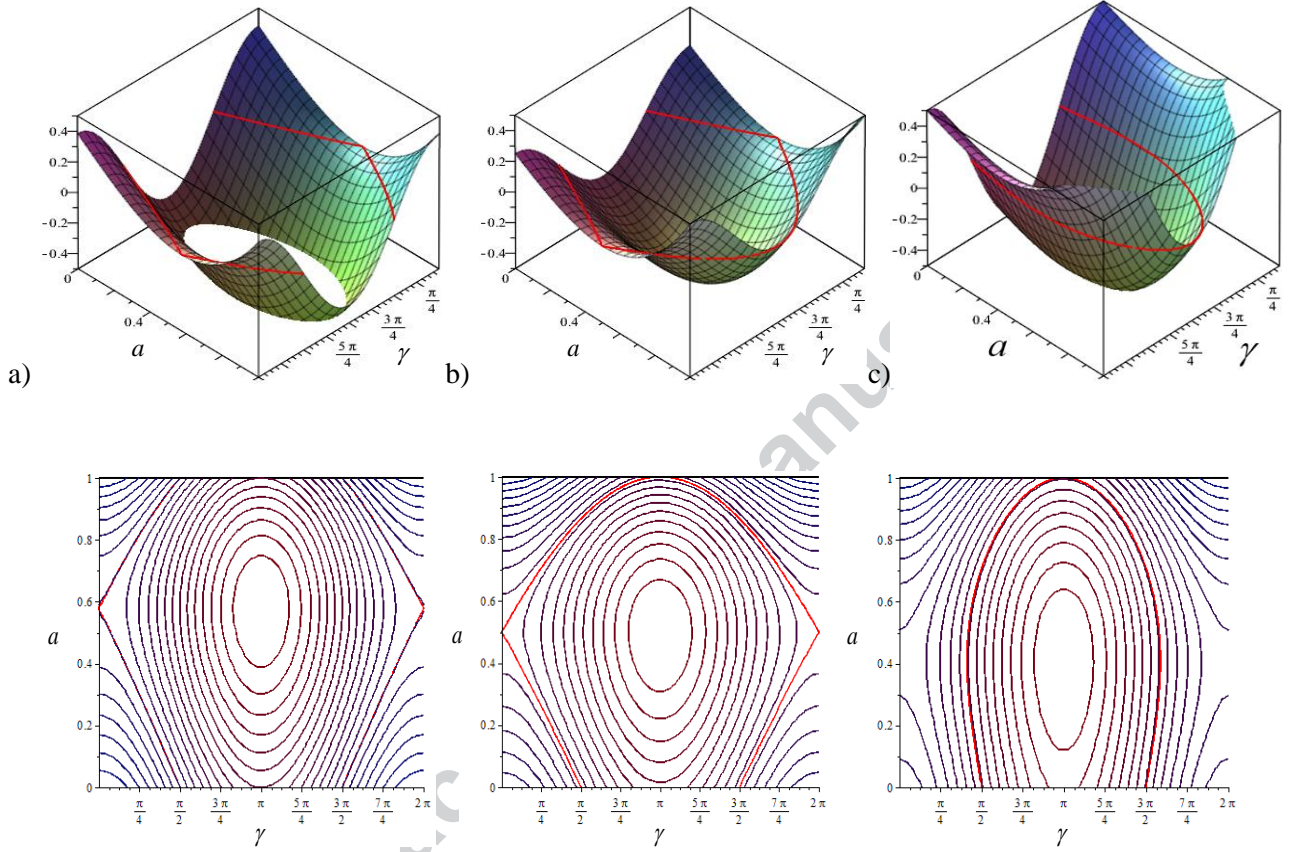

Figure 10- 3D and 2D projections of the system's RM, for $\eta = 1$; a) pure saddle mechanism, for $\sigma = -2, f = 0.7698$, b) co-existance of both escape mechanisms, for $\sigma = -1.5, f = 0.5$, c) pure maximum mechanism, for $\sigma = -1, f = 1$.

The analytical approach used above is based on the integrability of the corresponding Hamiltonian case of the original system in Equation (36), and hence cannot involve the dissipative terms. Naturally, another approach should be adopted herein in order to consider the quantitative change of the RM due to damping. In the following section, correction terms will be found for each escape mechanism, under the assumption of small damping.

5.1.2. Escape through saddle mechanism

Despite the lack of integrabiliy, the phase plane of the slow-evolution equations (36), have the same dimensionality as in the conservative case. When small damping is added, i.e. $(0 < \varepsilon\lambda \ll 1)$, the RM undergoes a continuous change, in which both escape mechanisms are preserved.

The corrected location of the saddle point in the perturbed case is obtained by the following series expansion:

$$a_s = a_{S,0} + \varepsilon\lambda a_{S,1} + O\left(\varepsilon^{3/2}\right), \; \gamma_s = \varepsilon\lambda\gamma_{S,1} + O\left(\varepsilon^{3/2}\right) \tag{44}$$

Phase trajectory originating at $a(0) = 0, \gamma(0) = \pi/2$ will hit this saddle point, if the forcing is a bit higher than the critical forcing for the undamped case:

$$f_{cr,S} = f_{cr,S,0} + \varepsilon\lambda f_{cr,S,1} + O\left(\varepsilon^{3/2}\right) \tag{45}$$

The problem lies in finding the correction for the critical forcing, $\varepsilon\lambda f_{cr,S,1}$ for fixed values of η, σ. To achieve this goal, we can study the evolution of function $H(a, \gamma, f)$, when the system is described by **complete slow** evolution equations in Equation (36):

$$\frac{d}{d\tau} H(a, \gamma, f) = \frac{\partial H}{\partial a}\varepsilon a' + \frac{\partial H}{\partial \gamma}\varepsilon\gamma' = -\frac{\varepsilon\lambda a}{2}\left(4\eta a^3 + \sigma a + \frac{f}{2}\cos\gamma\right) \tag{46}$$

The phase trajectory, as in the Hamiltonian case, originates at $a(0) = 0, \gamma(0) = \pi/2$ and terminates in the saddle point (a_S, γ_S). Thus, the value of the function $H(a, \gamma, f)$ at the saddle point is evaluated as follows:

$$H(a_S, \gamma_S, f) = -\frac{\varepsilon\lambda}{2}\int_0^\infty a(\tau)\left(4\eta a(\tau)^3 + \sigma a(\tau) + \frac{f}{2}\cos\gamma(\tau)\right)d\tau \tag{47}$$

Equation (47) itself is of little use in generic case, since we have no way to know the functions $a(\tau), \gamma(\tau)$. However, one notes that the right-hand side of Equation (47) is already of order $O(\varepsilon)$, and thus for $f = f_{cr,S,0} + \varepsilon\lambda f_{cr,S,1} + O\left(\varepsilon^{3/2}\right)$ one can evaluate the integral in Equation (47) taking the functions $a_0(\tau), \gamma_0(\tau)$ from the solution of the unperturbed/undamped problem, i.e. $\lambda = 0$, with zero initial conditions, $D = 0$. According to Equation (36) and Equation (40), those functions satisfy the following equations:

$$a_0' = \frac{f_{cr,0}}{2}\sin\gamma_0$$

$$a_0\gamma_0' = a_0\sigma + 4\eta a_0^3 + \frac{f_{cr,0}}{2}\cos\gamma_0 \tag{48}$$

$$\eta a_0^3 + \frac{\sigma}{2}a_0 + \frac{f_{cr,0}}{2}\cos\gamma_0 = 0$$

According to Equation (48), Equation (47) can be rewritten in the following form:

$$H(a_S, \gamma_S, f_{cr,S,0} + \varepsilon\lambda f_{cr,S,1}) = -\frac{\varepsilon\lambda}{2}\int_0^{a_0} \frac{a\left(3\eta a^3 + \frac{\sigma a}{2}\right)da}{\sqrt{\frac{f_{cr,S,0}^2}{4} - \left(\eta a^3 + \frac{\sigma a}{2}\right)^2}} + O\left(\varepsilon^{3/2}\right) \tag{49}$$

The integral in Equation (49) is evaluated with the help of the following substitution: $a^2 = \left(-\frac{\sigma}{6\eta}\right)x$.

$$H\left(a_S, \gamma_S, f_{cr,S,0} + \varepsilon\lambda f_{cr,S,1}\right) = -\frac{\varepsilon\lambda\sigma}{8\eta}\int_0^{x_0}\sqrt{\frac{x}{4-x}}dx + O\left(\varepsilon^{3/2}\right) = -\frac{\varepsilon\lambda\sigma}{8\eta}\left(\frac{2\pi}{3} - \sqrt{3}\right) + O\left(\varepsilon^{3/2}\right)$$

$$(50)$$

On the other hand, it is possible to evaluate the term $H(a_S, \gamma_S, f_{cr,S,0} + \varepsilon\lambda f_{cr,S,1})$ directly from Equation (40):

$$H(a_S, \gamma_S, f_{cr,S,0} + \varepsilon\lambda f_{cr,S,1}) = \frac{\varepsilon\lambda f_{cr,S,1} a_{S,0}}{2} + O(\varepsilon^{3/2}) \tag{51}$$

Thus, from Equations (50) and (51), one finally obtains the following correction for the critical forcing in the case of the saddle escape mechanism:

$$f_{cr,S,1} = \sqrt{-\frac{3\sigma}{2\eta}}\left(\frac{\pi}{3} - \frac{\sqrt{3}}{2}\right) \rightarrow f_{cr,S} = \frac{2}{3}\frac{(-\sigma)^{3/2}}{\sqrt{6\eta}} + \varepsilon\lambda\sqrt{-\frac{3\sigma}{2\eta}}\left(\frac{\pi}{3} - \frac{\sqrt{3}}{2}\right) + O(\varepsilon^{3/2}) \tag{52}$$

5.1.3. Escape through maximum mechanism

In this case, we assume that the phase trajectory originates at $a(0) = 0, \gamma(0) = \pi/2$ and terminates at the escape boundary of the RM $(a, \gamma) = (a_M, \gamma_M)$, where $a_M = 1$. Then, we perform a small perturbation with respect to the small damping parameter and the undamped escape point on the RM which corresponds to the maximum mechanism:

$$\gamma_M = \gamma_{M,0} + \varepsilon\lambda\gamma_{M,1} = \pi + \varepsilon\lambda\gamma_{M,1}$$
$$f_{cr,M} = f_{cr,M,0} + \varepsilon\lambda f_{cr,M,1} = \sigma + 2\eta + \varepsilon\lambda f_{cr,M,1} \tag{53}$$

Thus, the value of the function $H(a, \gamma, f)$ at the **maximum** point is evaluated as follows:

$$H(a_M, \gamma_M, f) = -\frac{\varepsilon\lambda}{2}\int_0^\infty a(\tau)\left(4\eta a(\tau)^3 + \sigma a(\tau) + \frac{f}{2}\cos\gamma(\tau)\right)d\tau \tag{54}$$

With account of Equation (48), Equation (54) can be rewritten in the following form:

$$H(a_M, \gamma_M, f_{cr,M}) = -\frac{\varepsilon\lambda}{2}\int_0^1 \frac{a\left(3\eta a^3 + \frac{\sigma a}{2}\right)da}{\sqrt{\left(\eta + \frac{\sigma}{2}\right)^2 - \left(\eta a^3 + \sigma a\right)^2}} = -\frac{\varepsilon\lambda}{2}\left(\frac{\xi}{2}I_1 + \frac{3}{2}I_2\right)$$

$$I_m = \int_0^1 \frac{t^m dt}{\sqrt{t(1-t)((t+\xi+1/2)^2 + \xi + 3/4)}}, m = 1, 2 \tag{55}$$

Here $\xi = \sigma/2\eta$ and $t = a^2$. The integrals in Equation (55) are radicals of the fourth degree and therefore can be reduced to Legendre normal forms [26]. For this sake, we introduce the following notation:

$$P = \sqrt{(\xi+3)(\xi+1)}, \ Q = \xi+1, \ \varphi = \frac{\sqrt{\xi+3} - \sqrt{\xi+1}}{\sqrt{\xi+3} + \sqrt{\xi+1}}, \ g = \frac{1}{(\xi+3)^{1/4}(\xi+1)^{3/4}}$$

$$k = \sqrt{\frac{1}{2} - \frac{2\xi^2 + 6\xi + 3}{4(\xi+3)^{1/2}(\xi+1)^{3/2}}} \tag{56}$$

Then, with the help of the notations in Equation (56), the integrals in Equation (55) are expressed as follows:

$$I_1 = \frac{2gQ}{Q-P}\left(\mathbf{K}(k) - \frac{1}{1-\varphi}\mathbf{\Pi}\left(\frac{\varphi^2}{\varphi^2-1},k\right)\right)$$

$$I_2 = \frac{2gQ^2}{(Q-P)^2}\left(\begin{array}{l}\dfrac{2\varphi}{\varphi-1}\mathbf{K}(k) - \left(\dfrac{2}{1-\varphi} + \dfrac{\varphi^2(2k^2-1)-2k^2}{(1-\varphi)^2(k^2+\varphi^2(1-k^2))}\right)\mathbf{\Pi}\left(\dfrac{\varphi^2}{\varphi^2-1},k\right) + \\[2mm] + \dfrac{\varphi^2(1+\varphi)}{(1-\varphi)(k^2+\varphi^2(1-k^2))}\mathbf{E}(k)\end{array}\right) \qquad (57)$$

Here $\mathbf{K}$, $\mathbf{E}$ and $\mathbf{\Pi}$ are complete elliptic integrals of the first, the second and the third kind respectively. The integrals exist for $\xi > -3/4$ and exhibit weak (logarithmic) singularity as $\xi \to -3/4$.

On the other hand, it is possible to evaluate $H(a_M, \gamma_M, f_{cr,M,0} + \varepsilon\lambda f_{cr,M,1})$ directly from Equation (40):

$$H(a_M, \gamma_M, f_{cr,M,0} + \varepsilon\lambda f_{cr,M,1}) = -\frac{\varepsilon\lambda}{2}f_{cr,M,1} + O\left(\varepsilon^{3/2}\right) \qquad (58)$$

Equating expressions (55) and (58), one obtains the correction term for the forcing amplitude:

$$f_{cr,M,1} = \frac{\xi}{2}I_1 + \frac{3}{2}I_2 \qquad (59)$$

The next subsection is devoted to numeric verifications of the corrections obtained for the escape thresholds through both escape mechanisms.

5.2. Numerical verification

5.2.2. Saddle mechanism

According to Equation (52), for parameters $\varepsilon = 0.1, \sigma = -2, \eta = 1, \lambda = 0.01$, the theoretical correction for the forcing amplitude should be as follows: $f_{cr,S,1} = \sqrt{3}\left(\pi/3 - \sqrt{3}/2\right) \approx 0.313799$.
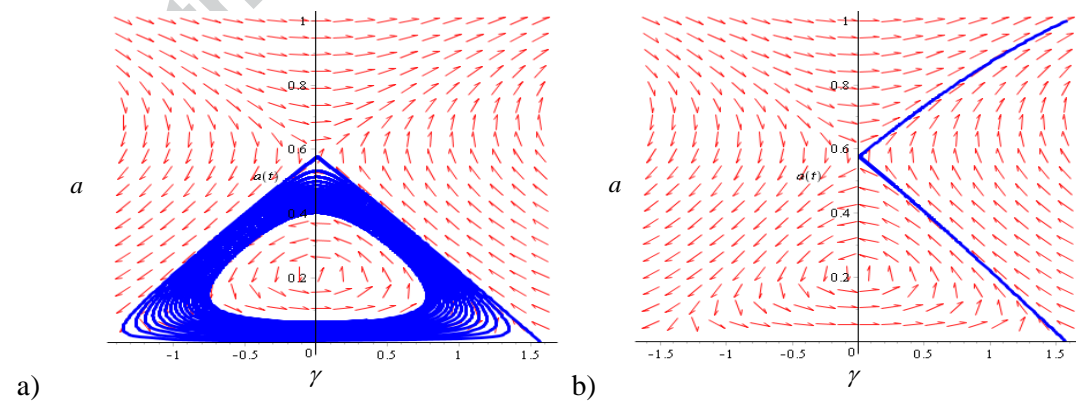

a)   b)

Figure 11 Phase flow portraits (red arrows) with numerical simulations (blue lines), which correspond to the slow-flow equations of the system in Equation (36), for $\varepsilon = 0.1, \sigma = -2, \eta = 1, \lambda = 0.1$; a) $f_{cr,S,1} = 0.313795$; b) $f_{cr,S,1} = 0.313796$

In Figure 11 (a) and (b), the system reaches the saddle point. Then, in the first case (Figure 11 (a)), the amplitude undergoes slow decay. On the other hand, in the second case (Figure 11 (b))

the amplitude rapidly increases to unity, leading to escape from the well. The numerical results are in excellent agreement with analytical predictions, with error of 0.001%.

5.2.1. Maximum mechanism

According to Equation (59), for parameters $\varepsilon = 0.1, \sigma = -1, \eta = 1, \lambda = 0.1$, the theoretical correction for the forcing amplitude should be as follows: $f_{cr,M,1} \approx 1.408408$. Numerical results show excellent agreement with the theoretical predictions, with error of 0.07%.
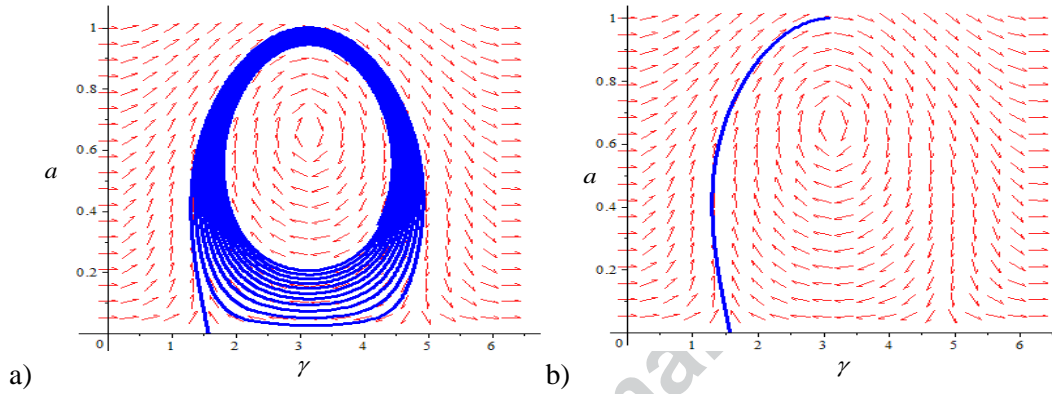

Figure 12- Phase flow portraits (red arrows) with numerical simulations (blue lines), which correspond to the slow-flow equations of the system (36), for $\varepsilon = 0.1, \sigma = -1, \eta = 1, \lambda = 0.1$,

$$a)\, f_{cr,M,1} = 1.4073966, \quad b)\, f_{cr,M,1} = 1.4073967$$

Numerical verification of the analytical prediction of the escape curve is shown in Figure 13. One can see that there is a good agreement between both the analytical and numerical results. Moreover, it is demonstrated that the sharp minimum still persists also in the weakly-damped case.
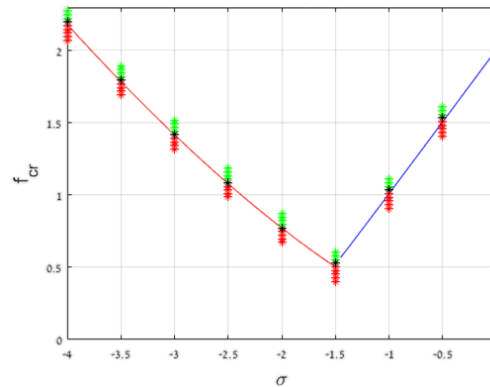

Figure 13- Comparison between asymptotic and numerical results of the perturbed escape curve. Red and blue lines correspond to the predicted escape thresholds associated with the saddle and maximum mechanisms, respectively. Red, green and black points correspond to no escape, escape, and escape threshold, respectively), for $\varepsilon = 0.1, \lambda = 0.1, \eta = 1$.

6. Conclusions

The results shown in the current paper deal with the escape problem of a tractable model of a classical harmonically forced damped particle in a truncated potential well. In the case of the parabolic truncated well, for non-zero damping values, the escape curve exhibits a smooth parabolic minimum. Moreover, for small damping values, the escape mechanism is governed by transient over-shoot behavior, and on the other hand, for large damping exceeding a critical value, the escape process is governed by the steady-state response.

However, when the parabolic truncated well is perturbed by weak quartic and cubic terms, the escape patterns undergo a qualitative modification. The escape process is dominated by two "competing" mechanisms, described by two intersecting independent branches of the escape curve. Their intersection leads to a sharp minimum ('dip'), shifted with respect to the natural frequency of the system. As one could expect, the quartic and cubic nonlinearities contribute opposite effects on the direction of shift of the curve minimum, due to their softening and hardening effects, respectively.

7. References

[1]   L. N. Virgin, "Approximate criterion for capsize based on deterministic dynamics," *Dyn. Stab. Syst.*, vol. 4, no. 1, pp. 56–70, Jan. 1989.

[2]   L. N. Virgin, R. H. Plaut, and C.-C. Cheng, "Prediction of escape from a potential well under harmonic excitation," *Int. J. Non. Linear. Mech.*, vol. 27, no. 3, pp. 357–365, May 1992.

[3]   G. Hunt and L. Virgin, "Michael Thompson: some personal recollections," *Philos. Trans. R. Soc. A Math. Phys. Eng. Sci.*, vol. 371, no. 1993, pp. 20120449–20120449, May 2013.

[4]   B. P. Mann, "Energy criterion for potential well escapes in a bistable magnetic pendulum," *J. Sound Vib.*, vol. 323, no. 3–5, pp. 864–876, Jun. 2009.

[5]   F. M. Alsaleem, M. I. Younis, and L. Ruzziconi, "An Experimental and Theoretical Investigation of Dynamic Pull-In in MEMS Resonators Actuated Electrostatically," *J. Microelectromechanical Syst.*, vol. 19, no. 4, pp. 794–806, Aug. 2010.

[6]   V. L. Belenky, N. B. Sevast′ianov, R. Bhattacharyya, and M. E. McCormick, *Stability and safety of ships : risk of capsizing*. Society of Naval Architects and Marine Engineers, 2007.

[7]   G. J. Simitses, "Instability of Dynamically-Loaded Structures," *Appl. Mech. Rev.*, vol. 40, no. 10, p. 1403, Oct. 1987.

[8]   R. Benzi, A. Sutera, and A. Vulpiani, "The mechanism of stochastic resonance," *J. Phys. A. Math. Gen.*, vol. 14, no. 11, pp. L453–L457, Nov. 1981.

[9]   L. Gammaitoni, P. Hänggi, P. Jung, and F. Marchesoni, "Stochastic resonance," *Rev. Mod. Phys.*, vol. 70, no. 1, pp. 223–287, Jan. 1998.

[10]   C. S. HSU, C.-T. KUO, and R. H. PLAUT, "Dynamic stability criteria for clamped shallow arches under timewisestep loads," *AIAA J.*, vol. 7, no. 10, pp. 1925–1931, Oct. 1969.

[11]   D. Dinkler and B. Kröplin, "Stability of Dynamically Loaded Structures," Springer, Berlin, Heidelberg, 1990, pp. 183–192.

[12] G. Rega and S. Lenci, "Dynamical Integrity and Control of Nonlinear Mechanical Oscillators," *J. Vib. Control*, vol. 14, no. 1–2, pp. 159–179, Jan. 2008.

[13] D. Orlando, P. B. Gonçalves, S. Lenci, and G. Rega, "Influence of the mechanics of escape on the instability of von Mises truss and its control," *Procedia Eng.*, vol. 199, pp. 778–783, Jan. 2017.

[14] L. Ruzziconi, A. M. Bataineh, M. I. Younis, W. Cui, and S. Lenci, "Nonlinear dynamics of an electrically actuated imperfect microbeam resonator: experimental investigation and reduced-order modeling," *J. Micromechanics Microengineering*, vol. 23, no. 7, p. 075012, Jul. 2013.

[15] O. V. Gendelman and L. I. Manevitch, *Tractable Models of Solid Mechanics: Formulation, Analysis and Interpretation*. Springer Science & Business Media, 2011.

[16] L. I. Manevitch and V. V. Smirnov, "Limiting phase trajectories and the origin of energy localization in nonlinear oscillatory chains," *Phys. Rev. E*, vol. 82, no. 3, p. 036602, Sep. 2010.

[17] L. I. Manevitch, A. S. Kovaleva, and D. S. Shepelev, "Non-smooth approximations of the limiting phase trajectories for the Duffing oscillator near 1:1 resonance," *Phys. D Nonlinear Phenom.*, vol. 240, no. 1, pp. 1–12, Jan. 2011.

[18] L. I. Manevitch and A. I. Musienko, "Limiting phase trajectories and energy exchange between anharmonic oscillator and external force," *Nonlinear Dyn.*, vol. 58, no. 4, pp. 633–642, Dec. 2009.

[19] O. V. Gendelman, "Escape of a harmonically forced particle from an infinite-range potential well: a transient resonance," *Nonlinear Dyn.*, vol. 93, no. 1, pp. 79–88, Jul. 2018.

[20] D. Naiger and O. V. Gendelman, "Escape dynamics of a forced- damped classical particle in an infinite- range potential well," *ZAMM - J. Appl. Math. Mech. / Zeitschrift für Angew. Math. und Mech.*, p. e201800298, Feb. 2019.

[21] O. V. Gendelman and G. Karmi, "Basic mechanisms of escape of a harmonically forced classical particle from a potential well," *Nonlinear Dyn.*, vol. 98, no. 4, pp. 2775–2792, Dec. 2019.

[22] M. Farid and O. V. Gendelman, "Escape of a forced-damped particle from weakly nonlinear truncated potential well," *arXiv Prepr. arXiv1910.08545*, Oct. 2019.

[23] O. V. Gendelman and T. P. Sapsis, "Energy Exchange and Localization in Essentially Nonlinear Oscillatory Systems: Canonical Formalism," *J. Appl. Mech.*, vol. 84, no. 1, p. 011009, Oct. 2016.

[24] M. Farid, "Escape of a harmonically forced classical particle from asymmetric potential well," *Commun. Nonlinear Sci. Numer. Simul.*, vol. 84, p. 105182, 2020.

[25] A. H. Nayfeh and D. T. Mook, *Nonlinear Oscillations*. John Wiley & Sons, 2008.

[26] P. F. Byrd and M. D. Friedman, *Handbook of Elliptic Integrals for Engineers and Scientists*. Springer, Berlin, Heidelberg, 1971.